INTERNATIONAL JOURNAL FOR NUMERICAL METHODS IN FLUIDS
Int. J. Numer. Meth. Fluids 2007; **54**:1387–1406
Published online 13 February 2007 in Wiley InterScience (www.interscience.wiley.com). DOI: 10.1002/fld.1411

A simplified v^2–f model for near-wall turbulence

M. M. Rahman*, † and T. Siikonen

Department of Mechanical Engineering, Laboratory of Applied Thermodynamics, Helsinki University of Technology, Sähkömiehentie 4, FIN-02015 HUT, Finland

SUMMARY

A simplified version of the v^2–f model is proposed that accounts for the distinct effects of low-Reynolds number and near-wall turbulence. It incorporates modified $C_{\varepsilon(1,2)}$ coefficients to amplify the level of dissipation in non-equilibrium flow regions, thus reducing the kinetic energy and length scale magnitudes to improve prediction of adverse pressure gradient flows, involving flow separation and reattachment. Unlike the conventional v^2–f, it requires one additional equation (i.e. the elliptic equation for the elliptic relaxation parameter f_μ) to be solved in conjunction with the k–ε model. The $\overline{v}^2$ scaling is evaluated from k in collaboration with an anisotropic coefficient C_v and f_μ. Consequently, the model needs no boundary condition on $\overline{v}^2$ and avoids free stream sensitivity. The model is validated against a few flow cases, yielding predictions in good agreement with the direct numerical simulation (DNS) and experimental data.

Received 19 July 2006; Revised 27 October 2006; Accepted 31 October 2006

KEY WORDS: v^2–f model; near-wall turbulence; elliptic relaxation; flow separation and reattachment

1. INTRODUCTION

An important criterion regarding the appropriateness of the turbulence model is to represent the near-wall behaviour of turbulence quantities accompanied by a preferential damping of velocity fluctuations in the direction normal to the wall that reconciles the influence of wall proximity adequately. In free flows, decreasing the local Reynolds number introduces only the viscous effect and the pressure fluctuations redistribute the kinetic energy on all components of the Reynolds stress tensor (and therefore return to isotropy effect). However, the transfer of energy from streamwise to the wall normal velocity fluctuations is suppressed by distant interaction of pressure fluctuations with the solid wall [1]. This effect combined with the molecular viscosity effect contributes to

*Correspondence to: M. M. Rahman, Department of Mechanical Engineering, Laboratory of Applied Thermodynamics, Helsinki University of Technology, Sähkömiehentie 4, FIN-02015 HUT, Finland.
†E-mail: mizanur.rahman@hut.fi

an increased anisotropy of turbulence near the wall, leading to wall blocking. Therefore, near-wall turbulence includes both viscous and blocking effects while low Reynolds number (LRN) turbulence consists of the viscous effect alone [2]. Consequently, the modification proposed for LRN turbulence is not necessarily applicable to near-wall flows.

In principle, the wall normal and shear stresses ($\overline{v}^2$, $-\overline{uv}$) are strongly damped in the near-wall region of a turbulent flow. Numerous variants of k–ε eddy viscosity models have been devised to mimic the turbulence attenuation accompanied by the proper behaviour of the eddy viscosity near the wall [2–18]. The standard k–ε model is devised for high Reynolds number turbulent flows and is traditionally used in wall-bounded flows in conjunction with a wall function approach to patch the core region of the flow to the wall region. Unfortunately, universal wall functions do not exist in complex flows having boundary-layer separation or complex alterations of the surface transport properties. Predictions of such flows with a high Reynolds number turbulence model can be degraded significantly when integrating to a solid boundary without the proper near-wall modifications. Consequently, the LRN modelling of turbulence has received extensive attention, rooted on the resolved turbulence transport processes in the vicinity of the wall. However, the isotropic LRN k–ε model associated with the viscous damping function and near-wall correction is not always sufficient to provide the appropriate velocity scale (i.e. $\sqrt{k}$ is the velocity scale in k–ε model) of turbulence, thus overpredicting the eddy viscosity. The possible reasoning is that $\overline{v}^2$ rather than k is the appropriate velocity scale towards the wall [19, 20]. Since the wall normal component $\overline{v}^2$, a key contributor to the mixing process, is severely damped in near-wall regions, the direct influence of the viscous damping function is avoided. The generalized interpretation of the velocity scale $\overline{v}^2$ can be found in Reference [21].

The v^2–f model suggested by Durbin [20] retains $\overline{v}^2$ and its source term f as variables in addition to the traditional k and ε parameters of the k–ε model. This enables to account for wall blocking akin to second-moment closures where all stress components are computed and the damping is achieved by blocking the energy redistribution with the pressure fluctuations. The quantity $\overline{v}^2$ is obtained from a transport equation simplified from the second-moment closure. The associated pressure–strain term in the $\overline{v}^2$ equation, responsible for redistribution of k in the proximity of walls in order to return the correct level of turbulence anisotropy, is obtained from an auxiliary elliptic equation for f which is the modified Helmholtz equation (the solution of which is close to an exponential decay as the wall is approached). Despite encouraging results of fluid flow problems encountered in engineering applications, the use of the model is complicated due to a removable singularity associated with the boundary condition for f. A code friendly version of the v^2–f model to abandon the singularity, in a way similar to the $\tilde{\varepsilon}$ change of variable by Reference [3] for the k–ε model, has been suggested by Lien and Durbin [22], allowing a segregated solution to the turbulence field. The model is not only numerically friendly but ideal for block-structured and unstructured grid methods including their parallelization [23]. Nevertheless, the introduced modifications lead to some deviations in certain flow regimes, compared with the original v^2–f model and both models exhibit free-stream dependency [24].

On the way of devising a simplified v^2–f model, the present study concentrates on LRN and near-wall turbulence for the isotropic k–ε model where the integration up to the wall is extremely important. Sticking to the conventional definition for μ_T, the v^2 equation is deduced using the eddy viscosity relationship of Reference [20] and imposing certain constraints. The wall blocking is governed by an elliptic partial differential equation (i.e. Helmholtz-type equation) and naturally, non-local near-wall effects are taken into account. The improvement herein springs principally from the modelling of the velocity scale $\overline{v}^2$ (as a product of the anisotropic coefficient C_v, elliptic

DOI: 10.1002/fld

relaxation function f_μ and k) to suppress the excessive eddy viscosity in near-wall regions. To this end, it must be emphasized that compared to the original and modified v^2–f models, the present formulation has the following attributes. It solves one additional equation in conjunction with the k–ε model, i.e. an elliptic equation for the elliptic relaxation parameter f_μ. The characteristic length scale associated with the elliptic relaxation equation is designed in terms of Kolmogorov and dynamic length scales in conjunction with the invariants of strain rate and vorticity tensors. Consequently, the large constant-dependent sensitivity of the relaxation function is reduced massively [20], and the non-local effects are explicitly influenced by the mean flow and turbulent variables. The model sensitivity to free stream values is absent and finally, the turbulence anisotropy is introduced with both the model coefficients $C_{\varepsilon(1,2)}$ and $\sigma_{(k,\varepsilon)}$.

The model performance is validated against experimental and DNS data of well-documented flows, consisting of a fully developed channel flow, a flat plate boundary layer flow with zero pressure gradient, a backward facing step flow, an asymmetric plane diffuser flow, and heat transfer from a semiconfined impinging round jet, respectively. Particular attention is paid to assess the capability of the new model, relative to the Lien and Durbin model (LDM), i.e. the code friendly variant of the v^2–f model, when used to predict the flows associated with transition, flow separation and reattachment. The test cases are selected such as to justify the ability of the models to replicate the combined effects of LRN, near-wall turbulence and non-equilibrium.

2. TURBULENCE MODELLING

In collaboration with the Reynolds-averaged Navier–Stokes (RANS) equations, the proposed model determines the turbulence kinetic energy k and its dissipation rate ε by the following transport relations:

$$\frac{\partial \rho k}{\partial t} + \frac{\partial \rho u_j k}{\partial x_j} = \frac{\partial}{\partial x_j}\left[\left(\mu + \frac{\mu_\mathrm{T}}{\sigma_k}\right)\frac{\partial k}{\partial x_j}\right] + \rho P - \rho\varepsilon \tag{1}$$

$$\frac{\partial \rho \varepsilon}{\partial t} + \frac{\partial \rho u_j \varepsilon}{\partial x_j} = \frac{\partial}{\partial x_j}\left[\left(\mu + \frac{\mu_\mathrm{T}}{\sigma_\varepsilon}\right)\frac{\partial \varepsilon}{\partial x_j}\right] + (C_{\varepsilon 1}\rho P - C_{\varepsilon 2}\rho\varepsilon)/T_t \tag{2}$$

where μ implies the molecular viscosity, $\sigma_{(k,\varepsilon)}$ are the appropriate turbulent Prandtl numbers and the production term $P = -\overline{u_i u_j}(\partial u_i/\partial x_j)$. The Reynolds stresses $\rho\overline{u_i u_j}$ are related to the mean strain-rate tensor S_{ij} through the Boussinesq approximation:

$$-\rho\overline{u_i u_j} = 2\mu_\mathrm{T}(S_{ij} - \tfrac{1}{3}S_{kk}\delta_{ij}) - \tfrac{2}{3}\rho k\delta_{ij} \tag{3}$$

Since the viscous dissipation presumably dominates near the wall, the turbulent viscosity is evaluated from [20]

$$\mu_\mathrm{T} = C_\mu \rho \overline{v}^2 T_t \tag{4}$$

where C_μ is a constant. The dynamic time scale k/ε is replaced by a realizable time scale T_t and can simply be defined as [20]

$$T_t = \sqrt{\frac{k^2}{\varepsilon^2} + C_\mathrm{T}^2\frac{\nu}{\varepsilon}} = \frac{k}{\varepsilon}\sqrt{1 + \frac{C_\mathrm{T}^2}{Re_\mathrm{T}}}, \quad Re_\mathrm{T} = \frac{k^2}{\nu\varepsilon} \tag{5}$$

DOI: 10.1002/fld

where $\nu = \mu/\rho$ denotes the kinematic viscosity and Re_T is the turbulence Reynolds number. Equation (5) warrants that the eddy time scale never falls below the Kolmogorov time scale $C_T\sqrt{\nu/\varepsilon}$, dominant in the immediate neighbourhood of the solid wall. It prevents the singularity in the dissipation equation down to the wall. Alternatively, the turbulence time scale is k/ε at large Re_T but approaches the Kolmogorov limit $C_T\sqrt{\nu/\varepsilon}$ for $Re_T \ll 1$. The empirical constant $C_T = 6$ associated with the Kolmogorov time scale is estimated from the DNS data for developed channel flows [20]. Obviously, the inclusion of T_t in the ε equation guarantees near-wall asymptotic consistency without resorting to *ad hoc* damping functions employed in many k–ε models [6]. The associated empirical functions/constants and the modelling of $\overline{v}^2$ are discussed in some detail in subsequent sections.

2.1. Code friendly variant of v^2–f model

The code friendly version appears with recourse to the removal of numerical oscillations/divergence mainly encountered when a segregated numerical procedure is adopted which does not allow an implicit coupling between $\overline{v}^2$ and f at the wall. According to the LDM [22], the change of the variable f is as follows:

$$f = \tilde{f} - 5\varepsilon\frac{\overline{v}^2}{k^2} = \tilde{f} - \frac{5}{T_t}\frac{\overline{v}^2}{k} \tag{6}$$

Unlike the original v^2–f model, the boundary condition for $\tilde{f} = 0$ at the wall, reducing the dependence between variables and greatly enhancing the numerical stability. Inserting Equation (6) into the original model provides for the new sets of relations:

$$\frac{\partial\rho\overline{v}^2}{\partial t} + \frac{\partial\rho U_j\overline{v}^2}{\partial x_j} = \rho k\tilde{f} - 6\rho\frac{\overline{v}^2}{T_t} + \frac{\partial}{\partial x_j}\left[\left(\mu + \frac{\mu_T}{\sigma_k}\right)\frac{\partial\overline{v}^2}{\partial x_j}\right] \tag{7}$$

$$-L^2\nabla^2\tilde{f} + \tilde{f} = \frac{1}{T_t}\left[(6 - C_1)\frac{\overline{v}^2}{k} + \frac{2}{3}(C_1 - 1) + C_2\frac{P}{\varepsilon}\right] \tag{8}$$

The modification retains the same asymptotic near-wall behaviour of $\overline{v}^2$ as in the original model: as $y \to 0$, $\overline{v}^2 \sim y^4$. As $y \to \infty$, the kinematic blocking stemming from the elliptic relaxation disappears. To this end, it must be acknowledged that the term $5L^2\nabla^2\overline{v}^2/(kT_t)$ which appears in the transformed $\tilde{f}$ equation is neglected, probably for the sake of gaining some privilege over numerical computation. However, this approximation lacks in theoretical justification. With the usual log-layer assumption for a developed channel flow (where $\overline{v}^2$ and k constant, $L \sim y$, $\varepsilon \sim 1/y$) the term $5L^2\nabla^2\overline{v}^2/(kT_t) \sim 1/y$, and hence it is a non-vanishing term in the $\tilde{f}$ equation.

Since the boundary conditions for both $\overline{v}^2 = 0$ and $\tilde{f}$ are homogeneous at the wall, the decoupling of $\overline{v}^2$ and $\tilde{f}$ equations is readily possible. The characteristic length scale L in Equation (8) is computed such as to provide smoother switch between Kolmogorov and dynamic length scales

$$L^2 = C_L^2\left(\frac{k^3}{\varepsilon^2} + C_\eta^2\sqrt{\frac{\nu^3}{\varepsilon}}\right) \tag{9}$$

DOI: 10.1002/fld

The change of variable forces the change in the definition of the coefficient $C_{\varepsilon 1}$ which is suited to feel the proximity of the wall [23]

$$C_{\varepsilon 1} = 1.4\left(1 + 0.05\sqrt{\frac{k}{\overline{v}^2}}\right) \tag{10}$$

It expedites a beneficial increase of ε near the edge of the sublayer with no explicit reference to the wall distance used in the previous version. The constants associated with the LDM are given by [23]

$$\begin{aligned} &C_\mu = 0.22, \quad \sigma_k = 1, \quad \sigma_\varepsilon = 1.3, \quad C_{\varepsilon 2} = 1.9 \\ &C_1 = 1.4, \quad C_2 = 0.3, \quad C_{\mathrm{L}} = 0.23, \quad C_\eta = 70 \end{aligned} \tag{11}$$

Noteworthily, Equation (8) can be solved using a tridiagonal matrix algorithm (TDMA) with an initial guess

$$\tilde{f} = \frac{1}{T_t}\left[(6 - C_1)\frac{\overline{v}^2}{k} + \frac{2}{3}(C_1 - 1) + C_2\frac{P}{\varepsilon}\right] \tag{12}$$

everywhere except on wall boundaries where $\tilde{f} = 0$. Kalitzin [24] conducted an analysis on the free-stream behaviour of the v^2–f model, demonstrating that under certain flow conditions the model provides a negative solution to the energy components in the free-stream region. There are several (arbitrary) ways to eliminate the undesirable sensitivity to the free-stream values, pertaining to the turbulence variables. The simplest way is to define a large value for the eddy viscosity at the inlet. At this stage, the price for avoiding the free-stream dependency is recommended as follows:

$$k = \max\left(k, \frac{\mu}{100}\frac{U_{\mathrm{ref}}}{\rho L_{\mathrm{ref}}}\right), \quad \mu_{\mathrm{T}} = \max\left(C_\mu \rho \overline{v}^2 T_t, \frac{\mu}{100}\right) \tag{13}$$

where L_{ref} and U_{ref} are the reference length and velocity, respectively. The $\overline{v}^2$ scaling is calculated as $\overline{v}^2 = \mu_{\mathrm{T}}/(C_\mu \rho T_t)$ in order to compute the convection–diffusion fluxes of Equation (7). In this manner, the lower bound on $\overline{v}^2$ is abandoned in favour of Equation (13).

2.2. *Simplified v^2–f model*

The evaluation of combined effects relating to LRN and near-wall turbulence (i.e. viscous and blocking effects) can be accelerated by introducing appropriate anisotropy together with the elliptic relaxation in the eddy viscosity formulation. The purpose herein is to construct a simplified v^2–f model with greater flexibility and increased accuracy in a manner similar to the LDM. To facilitate the subsequent development, the calculation commences by resorting to fully developed channel flows where the definition of the eddy viscosity yields [7]

$$\mu_{\mathrm{T}} = -\frac{\rho\overline{uv}}{\partial_y u} \tag{14}$$

However, most of the linear LRN k–ε models contain a viscous damping function f_μ in the eddy viscosity expression [6]

$$\mu_{\mathrm{T}} = C_\mu f_\mu \rho k T_t \tag{15}$$

DOI: 10.1002/fld

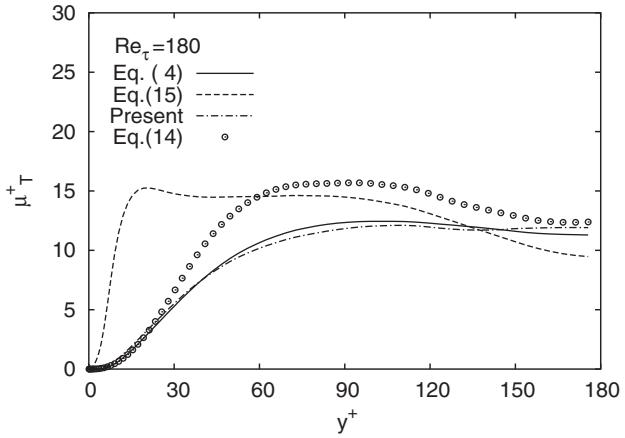

Figure 1. Exact eddy viscosity compared with k–ε and v^2–f models in wall co-ordinates.

The usual value of $C_\mu = 0.09$. The adopted form of f_μ corrects the asymptotic behaviour of μ_T, involving the distinct effects of LRN and wall proximity. In addition, $f_\mu = 1$ remote from the wall to ensure that the model is compatible with the standard k–ε turbulence model. Alternatively, the empirical function f_μ is valid in the whole flow field, including the viscous sublayer and the logarithmic layer.

Figure 1 shows the turbulent viscosity profiles constructed from the DNS data [25]. In this figure, Equation (4) is with the present value of $C_\mu = 0.2$ and Equation (15) assumes $f_\mu = 1$ (i.e. standard k–ε model). Comparing Equation (4) with Equation (14) reveals that the suppression of μ_T near the wall is largely accounted for by the $\overline{v}^2$ scaling, representing the anisotropy of near-wall turbulence. Relative to Equation (14), the k–ε model with $f_\mu = 1$ has the wrong profile in the near-wall region, clarifying the role of the damping function to fit the data with an expected curve near the wall. Nevertheless, the approach based on *ad hoc* tuning of f_μ is unattractive and fundamentally incorrect. The damping function is often nonlinear and may cause numerical stiffness. Its application is questionable in the presence of complex geometries and sophisticated problem statements.

Since the primary objective of introducing the damping effect to closure models is to represent the kinematic blocking by the wall, $\overline{v}^2$ rather than k is the appropriate velocity scale to use in the eddy viscosity formulation [20]. Presuming that Equations (4) and (15) are identical, and hence the following formula is obtained for $\overline{v}^2$:

$$\overline{v}^2 = C_v f_\mu k \tag{16}$$

where $C_v = 0.09/0.2 = 0.45$. Intuitively, the quantity $C_v f_\mu$ is responsible for the redistribution of turbulence kinetic energy in near-wall regions in order to return the correct level of turbulence anisotropy. Consequently, the constant value for C_v is avoided due to the following reasons: to reproduce the anisotropy of near-wall turbulence; to reduce the large constant-dependent sensitivity associated with the Kolmogorov length scale in the elliptic relaxation equation for f_μ defined afterwards; and finally, to influence the solution stability. The model coefficient C_v is assumed to be a scalar function of the invariants formed on the strain rate S_{ij} and vorticity W_{ij} tensors in

DOI: 10.1002/fld

question

$$S_{ij} = \frac{1}{2}\left(\frac{\partial u_i}{\partial x_j} + \frac{\partial u_j}{\partial x_i}\right), \quad W_{ij} = \frac{1}{2}\left(\frac{\partial u_i}{\partial x_j} - \frac{\partial u_j}{\partial x_i}\right) \tag{17}$$

The detailed functional form of C_v is determined relying on the constraints such as DNS and appropriate experiments, collaborated with the elliptic relaxation equation

$$C_v = \min\left[\frac{2}{3}, \sqrt{\frac{2}{3(1+\eta)}}\right], \quad \eta = T_t\sqrt{S_{ij}S_{ij} + W_{ij}W_{ij}} \tag{18}$$

It can be emphasized herein that the proposed relation indubitably is conducive to allowing compatible changes in C_v that account for the above-mentioned obviously desirable aspects. Apparently, at $\eta = 2.3$ Equation (18) is prone to recover $C_v \approx 0.45$.

Detailed analysis of DNS data shows that the kinematic blocking effect is much stronger than the viscous/LRN effect [26]. The empirical approach to modelling the wall-blocking effect is often inconsistent with the complex flows and may degrade the results considerably. In such a situation, the model usually includes some compensation for it, for instance, some additional source term in the ε equation. To eradicate the empiricism/complexity, a Helmholtz-type elliptic relaxation equation for f_μ is introduced. It represents a general ellipticity, pertaining to f_μ without the knowledge of the wall distance:

$$-L^2\nabla^2 f_\mu + f_\mu = 1 \tag{19}$$

where L is the characteristic length scale. To avoid the singularity close to the wall, the Kolmogorov length scale $(v^3/\varepsilon)^{1/4}$ is added to the dynamic length scale $k^{3/2}/\varepsilon$. After some manipulations, a compatibility relation is deduced as

$$L^2 = vC_\mu\left(C_\mu Re_T\frac{k}{\varepsilon} + C_\eta^2\sqrt{\frac{v}{\varepsilon}}\right), \quad C_\eta = C_T\sqrt{3C_T + \eta^2} \tag{20}$$

The rationale of the present approach is that the wall proximity effect is modelled naturally in conjunction with the elliptic relaxation function f_μ and hence non-local effects such as wall blocking. The virtue of Equation (19) is that unlike the Poisson equation, it requires no special numerical treatment. It can be solved in parallel with the k–ε equations having an initial guess $0 \leqslant f_\mu \leqslant 1$ everywhere except on wall boundaries where $f_\mu = 0$. With the DNS data Equation (19) is solved using a tridiagonal matrix algorithm (TDMA) to evaluate Equation (16). Substituting the result in Equation (4) supplies the eddy viscosity, plotted in Figure 1. Good correlation between the present and the data is obtained.

Noteworthily, with $\eta = 0$ (for instance, in the centre of a fully developed channel flow for an enough high *Re* number) $f_\mu = 1.0$ and the ratio $\overline{v}^2/k$ is forced to be $\frac{2}{3}$, approaching the isotropic turbulence where the ratio must be $\frac{2}{3}$. Thus, the present formulation confirms that $\overline{v}^2$ contains the average energy. To this end, it must be stressed that the present model determines the energy partition $\overline{v}^2/k$ by the length scale L in association with the anisotropic coefficient C_v, but not by the redistribution effect as is introduced with the LDM. In principle, the whole flow domain of the elliptic Helmholtz equation (8) is influenced by the walls and the solution of (8) relaxes to the homogeneous one far from the wall that is represented by the RHS of the equation. Hence, the

DOI: 10.1002/fld

proposal of the LDM can be thought of as an interpolation method between near-wall and free turbulence, with the interpolation coefficient provided by a non-local model. The present formulation is essentially contrived to replicate non-local effects in a slightly different manner, much the same as the LDM.

Near-wall flows show a tendency to underestimate the dissipation rate ε due to the local anisotropy of turbulence, adhering to the non-dimensional parameter P/ε [27]. Researchers allow the coefficient $C_{\varepsilon 1}$ to be a function of P/ε with a view to enhancing dissipation in such a situation [28, 29]. However, in some of the more complex flows that have been calculated, the dependence on P/ε prevents numerical convergence to a steady state [21]. One possible approach to counteracting this adverse situation is to explore alternative elements with relevance to P/ε:

$$C_{\varepsilon 1} = 1 + \sqrt{\frac{\overline{v}^2}{k}}, \quad C_{\varepsilon 2} = 1.27 C_{\varepsilon 1} \tag{21}$$

As $\overline{v}^2$ decreases faster than k in the near-wall region, the difference $(C_{\varepsilon 2} - C_{\varepsilon 1})$ becomes smaller thus accounting for the additional production of dissipation by the anisotropy of turbulence. The parameter P/ε is supposed to serve the same purpose when included with $C_{\varepsilon(1,2)}$.

The budgets of k and ε from the DNS data suggest that the role of turbulent diffusion in the near-wall region is substantial. Accordingly, the coefficients $\sigma_{(k,\varepsilon)}$ are modelled, rather than being assigned constant values (unlike the commonly adopted practice with $\sigma_k = 1.0$ and $\sigma_\varepsilon = 1.3$):

$$\sigma_k = C_\mu + \sqrt{\frac{\overline{v}^2}{k}}, \quad \sigma_\varepsilon = C_\mu^{2/3} + \sqrt{\frac{\overline{v}^2}{k}} \tag{22}$$

The model coefficients $\sigma_{(k,\varepsilon)}$ are developed such that sufficient diffusion is obtained in the vicinity of the wall. Equation (16) together with Equations (18) and (19) dictates that the turbulent Prandtl numbers $\sigma_{(k,\varepsilon)}$ have the values in the range from $C_\mu = 0.2$ to $(1 + C_\mu)$.

The transport equations for k and ε are subjected to the following boundary conditions at solid walls:

$$k_w = 0, \quad \varepsilon_w = 2\nu \left(\frac{\partial \sqrt{k}}{\partial y} \right)^2 \approx 2\nu \frac{k}{y^2} \tag{23}$$

To avoid numerical instability, the approximation for ε_w is applied at the first grid node neighbouring the wall, rather than on the wall itself. This requires normal distance from a wall to the nearest grid point, which is unambiguous and readily available. The validity of Equation (23) necessitates that the grid system is fine enough to produce the near-wall limiting behaviour.

3. COMPUTATIONS

To ascertain the efficacy of the proposed model, a few applications to the two-dimensional turbulent flows consisting of a fully developed channel flow, a flat plate boundary layer flow with zero pressure gradient, a backward facing step flow, an asymmetric plane diffuser flow, and heat transfer from a semiconfined impinging round jet are considered. For comparison purpose, calculations from the LDM [22] are included. The possible reasoning for the choice of the LDM lies mainly in its enhanced numerical stability compared to the original v^2–f model [20].

DOI: 10.1002/fld

A cell centred finite-volume scheme combined with an artificial compressibility approach is employed to solve the flow equations [30, 31]. A fully upwinded second-order spatial differencing is applied to approximate the convective terms. Roe's [32] damping term is used to calculate the flux on the cell face. A diagonally dominant alternating direction implicit (DDADI) time integration method [33] is applied for the iterative solution to the discretized equations. A multigrid method is utilized for the acceleration of convergence [34]. The basic implementation of the artificial compressibility method and associated features are described in [30, 31]. Note that the elliptic relaxation Equations (8) and (19) are solved using TDMA. In every co-ordinate direction, the implicit stage performs typically two sweeps that provide convincingly the converged state for $(\tilde{f},\ f_\mu)$ at each iteration level.

A variable grid spacing is used to resolve the sharp gradient in near-wall regions. Grid densities are varied to ensure the grid independence of the numerical results. It is found that the solution is not very sensitive to the number of grid points as long as there are two points in $y^+<1.5$. In the computations that follow, convergence is judged by monitoring the root-mean-square residuals of flow variables. The solution is taken as having converged when all the residuals are of the order 10^{-4} or less.

3.1. Channel flow

The computation is carried out for a fully developed turbulent channel flow at $Re_\tau = 395$ for which turbulence quantities are attainable from the DNS data [25]. Calculations are conducted in the half-width of the channel, imposing periodic boundary conditions except for the pressure, pertaining to the upstream and downstream boundaries. The computation involving a 64×48 non-uniform grid refinement is considered to be sufficiently accurate to describe the flow characteristics. The length of the computational domain is 32δ, where δ is the channel half-width. To ensure the resolution of the viscous sublayer, the first grid node near the wall is placed at $y^+ \approx 0.3$. Comparisons are made by plotting the results in the form of $u^+ = u/u_\tau$, $k^+ = k/u_\tau^2$, $\overline{v}^{+2} = \overline{v}^2/u_\tau^2$ and $\varepsilon^+ = \nu\varepsilon/u_\tau^4$ *versus* y^+.

Figure 2 shows the velocity profiles for different models. The prediction of the present model agrees well with the DNS data. The LDM slightly overestimates the mean velocity profile in the

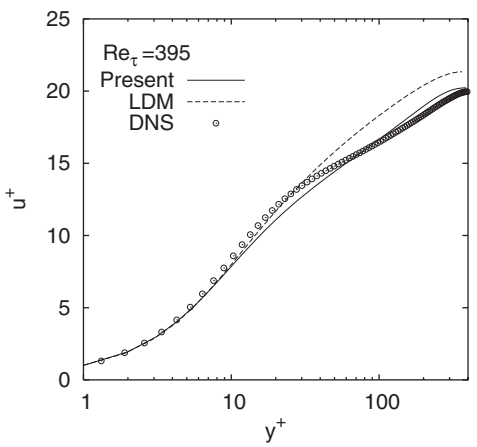

Figure 2. Mean velocity profiles of channel flow at $Re_\tau = 395$.

DOI: 10.1002/fld

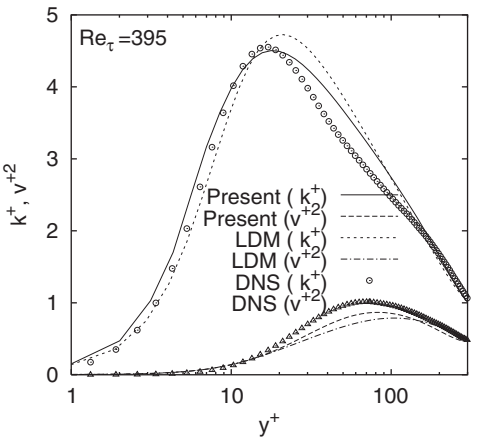

Figure 3. Turbulence kinetic energy and $\overline{v}^2$ profiles of channel flow at $Re_\tau = 395$.

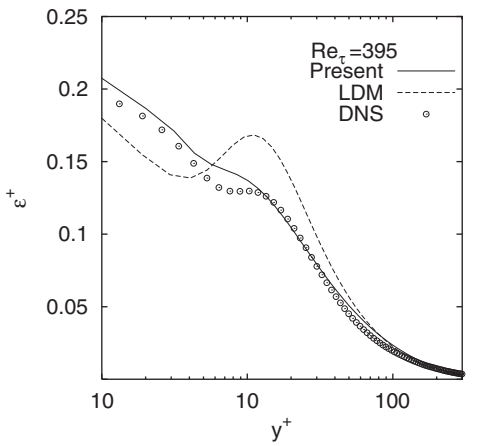

Figure 4. Dissipation rate profiles of channel flow at $Re_\tau = 395$.

outer layer. Further examination of the model performances is directed to the $(\overline{v}^{+2}, k^+)$ profiles as portrayed in Figure 3 for the near-wall region. As is evident, the present model prediction is in broad accord with the LDM and DNS data. Figure 4 exhibits the profiles of ε^+ from the two computations. The present as well as the LDM provides a maximum ε^+ at the wall which is more in line with the DNS data. However, agreement of the present model predictions with the DNS data seems to be satisfactory.

3.2. Flat plate boundary layer flow

The performance of the proposed model is further contrasted with the experimental data of the flow over a flat plate with a high free stream turbulence intensity. The test case is taken from

DOI: 10.1002/fld

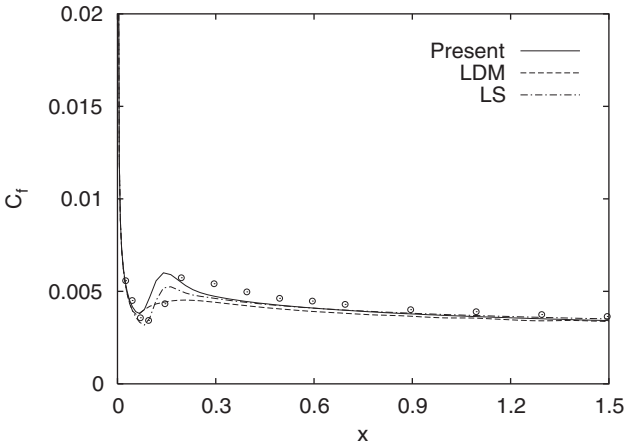

Figure 5. Streamwise skin friction coefficient of boundary layer flow.

'ERCOFTAC' Fluid Dynamics Database WWW Services (http://fluindigo.mech.surrey.ac.uk/) preserved by P. Voke. Measurements down to $x = 1.495$ m which corresponds to $Re_x \approx 94\,000$, are made by J. Coupland at Rolls-Royce. The inlet velocity is 9.4 m/s and the pressure gradient is zero. The upstream turbulence intensity $T_u = 6.0\%$, defined as $T_u = \sqrt{\frac{2}{3}k}/U_{ref}$, where U_{ref} indicates the reference (inlet) velocity. The dissipation is set so that the decay of free stream turbulence is in balance [13].

Computations begin 16 cm ahead of the leading edge and symmetric conditions are applied. The length and height of the grid are 1.6 and 0.3 m, respectively. The near-wall grid node is located at $y^+ < 1.0$, except the point at the leading edge ($y^+ = 2.1$). The grid size is 96×64 and heavily clustered near the wall.

The predicted skin friction coefficients ($C_f = 2u_\tau^2/U_{ref}^2$) are compared with the experimental data in Figure 5. Savill's investigation [35] approves that the Launder and Sharma (LS) model is one of the best models for the prediction of transition points. Therefore, the LS model [4] computation is plotted for comparison. All models exhibit an interesting feature that the transition starts at the right position and it is strong enough. Both the LS and present models return the skin friction in terms of its magnitude and trend with satisfactory accuracy. However, the LDM prediction is somewhat on a lower level than the data shown.

3.3. Backward facing step flow

To ascertain the performance in complex separated and reattaching turbulent flows, the present model is applied to the flow over a backward facing step. The computations are conducted corresponding to the experimental case with zero deflection of the wall opposite to the step, as investigated by Driver and Seegmiller [36]. The reference velocity $U_{ref} = 44.2$ m/s and the step height $h = 0.0127$ m. The ratio between the channel height and the step height is 9 and the step height Reynolds number is $Re = 3.75 \times 10^4$. At the channel inlet, the Reynolds number based on the momentum thickness is $Re_\theta = 5.0 \times 10^4$.

DOI: 10.1002/fld

For the computations, grids are arranged in two blocks. The smaller one (extended from the inlet to the step) contains a 16×48 non-uniform grid and the grid size for the other one is 120×80. The maximum height of the first near-wall grid node is at $y^+ < 1.5$. The inlet conditions are specified four step heights upstream of the step corner and the outlet boundary conditions are imposed 30 step heights downstream of the step corner. The inlet profiles for all dependent variables are generated by solving the models at the appropriate momentum thickness Reynolds number. All the quantities shown below are normalized by the step height h and the experimental reference free stream velocity U_{ref}, provided that the distance x/h is measured exactly from the step corner.

Computed and experimental friction coefficients C_{f} along the step side wall are plotted in Figure 6. As is observed, both models are in good agreement with the data. The positive C_{f} that

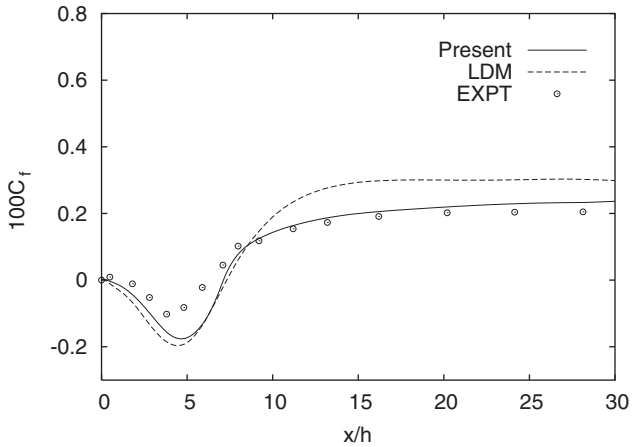

Figure 6. Skin friction coefficient along the step-side bottom wall.

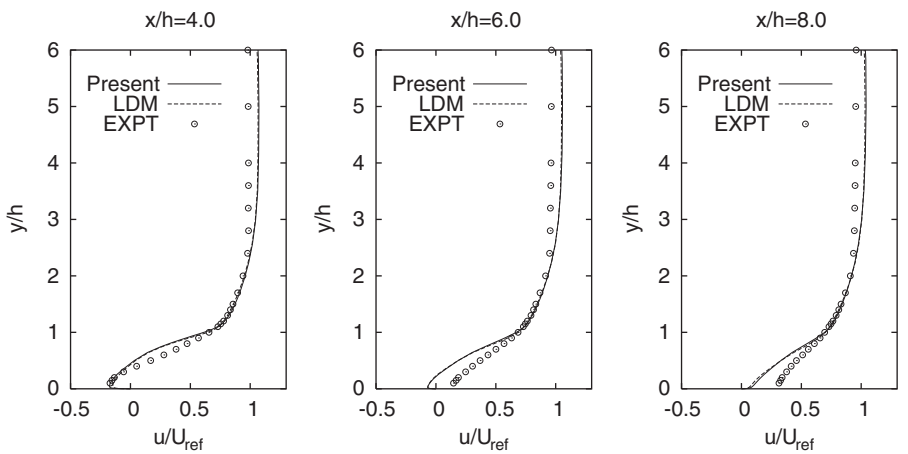

Figure 7. Mean velocity profiles at selected locations for step flow.

DOI: 10.1002/fld

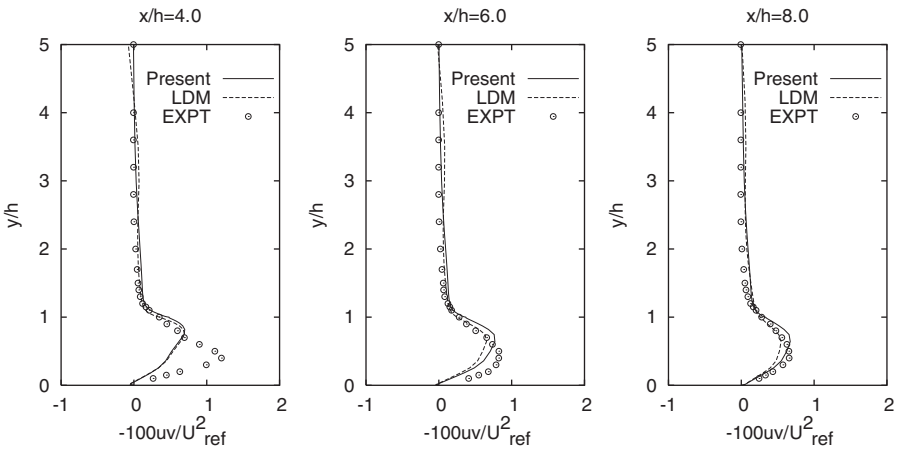

Figure 8. Shear stress profiles at selected locations for step flow.

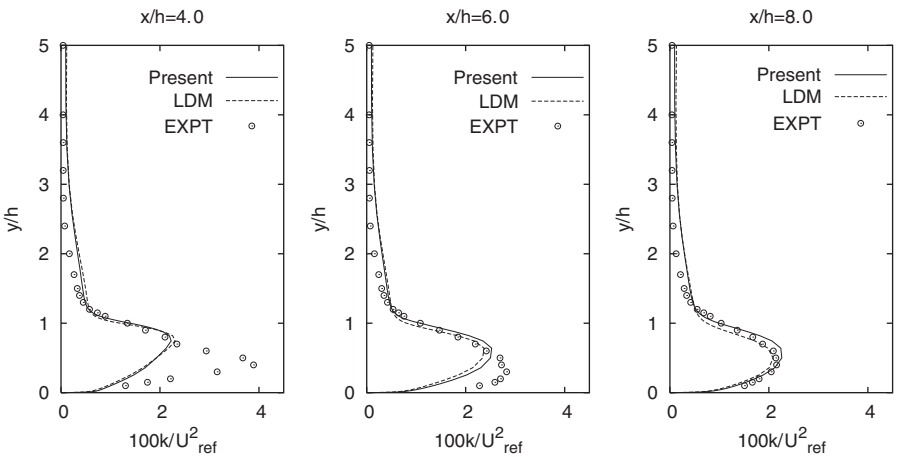

Figure 9. Kinetic energy profiles at selected locations for step flow.

starts from $x/h = 0$ is due to a secondary eddy which sits in the corner at the base of the step, inside the main recirculation region. The recirculation lengths predicted by the present and LDM models are 7.0 and 7.2 h, respectively. The experimental value of the reattachment length is 6.26 ± 0.1 h, making a fairly good correspondence with the models.

The streamwise mean velocity profiles at three representative positions are depicted in Figure 7. Obviously, the predictions of both models are in good agreement with the experiment. Comparisons are extended to the distributions of Reynolds shear stress and the corresponding turbulent kinetic energy at different x/h locations behind the step corner, as shown in Figures 8 and 9. A closer inspection of the distribution indicates that both model predictions have satisfactory agreement with the experimental data in both the recirculation and recovery regions.

DOI: 10.1002/fld

3.4. Asymmetric plane diffuser flow

To further validate the performance in complex separated and reattaching turbulent flows, the present model is applied to the flow in an asymmetric diffuser with an opening angle of 10°, for which measurements are available [37]. The expansion ratio of 4.7 is sufficient to produce a separation bubble on the deflected wall. Hence, the configuration provides a test case for smooth, adverse pressure-driven separation. The entrance to the diffuser consists of a plane channel to invoke fully developed flow with $Re = 2.0 \times 10^4$ based on the centreline velocity U_{ref} and the inlet channel height h. Computations involving a 120×72 non-uniform grid resolution are considered to be accurate to describe the flow characteristics. The length of the computational domain is 76 h. The thickness of the first cell remains below one in y^+ units on both the deflected and flat walls.

Figure 10 portrays the predicted skin friction coefficients C_{f}. The performance of the present model evinces an encouraging qualitative agreement with measurements. Figure 11 exhibits the

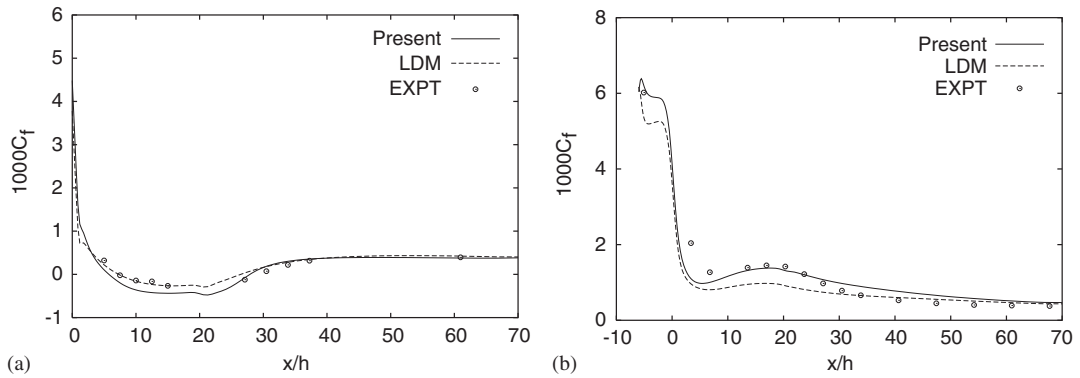

Figure 10. Skin friction coefficients of diffuser flow: (a) along the deflected bottom wall and; (b) along the straight top wall.

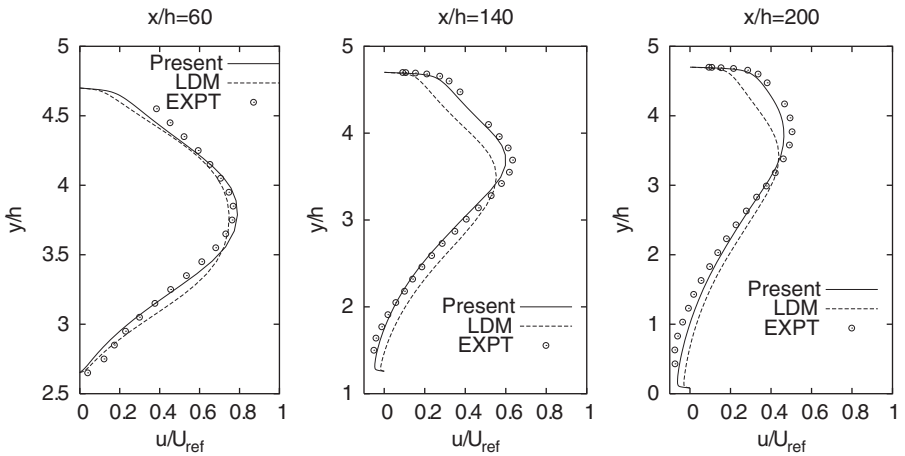

Figure 11. Mean velocity profiles at selected locations for diffuser flow.

DOI: 10.1002/fld

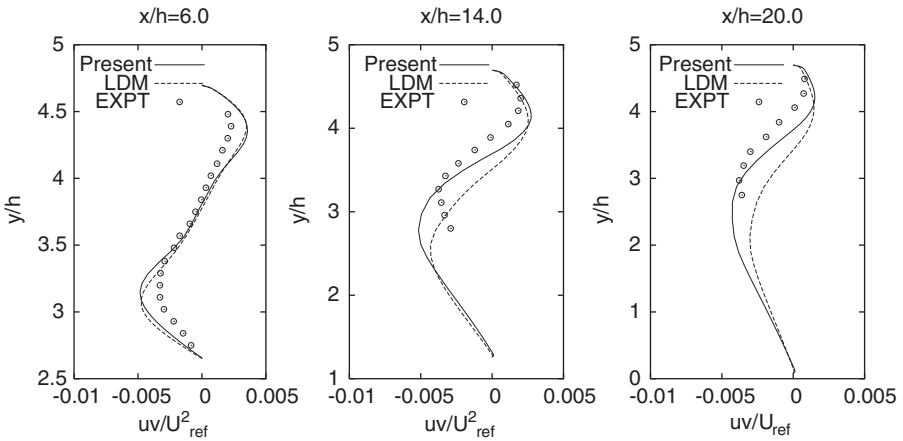

Figure 12. Shear stress profiles at selected locations for diffuser flow.

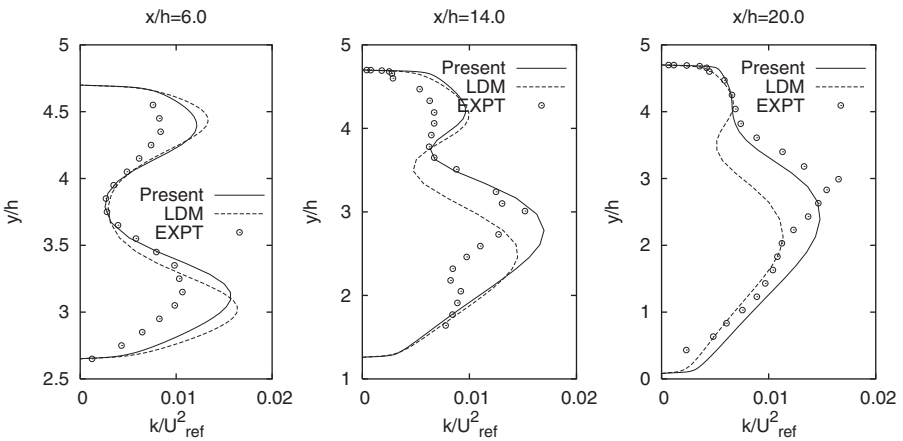

Figure 13. Kinetic energy profiles at selected locations for diffuser flow.

mean velocity profiles at three representative positions. The overall performance in predicting the velocity profiles is the best for the present model. Towards downstream of the diffuser the computed values of mean velocities, pertaining to the LDM become noticeably smaller than the data show, except near the wall.

Profiles of the shear stress at three representative streamwise positions are given in Figure 12. As is observed, the present model predictions are in broad accord with the measured data. The superiority of the proposed model over the LDM is once more ascertained. The comparisons of predicted and measured kinetic energy profiles are displayed in Figure 13 at various x/h locations. Reasonable agreement is achieved by the present model. On the other hand, the LDM has noticeable discrepancies with the measured data farther downstream.

DOI: 10.1002/fld

3.5. *Semiconfined impinging axisymmetric jet*

The performance of the proposed model is further contrasted with the experimental data of the turbulent axisymmetric jet impinging within a semiconfined space [38, 39]. The Reynolds number based on the nozzle diameter D is 2.0×10^4 and a nozzle to plate space is of two dimensions. The inlet velocity and turbulence kinetic energy are approximated from the experimental data. The inlet profile for the energy dissipation is evaluated from $\varepsilon = k^{1.5}/L$, where L is estimated to be 6% of the inlet diameter. A constant temperature is prescribed at the wall which simulates the experimental

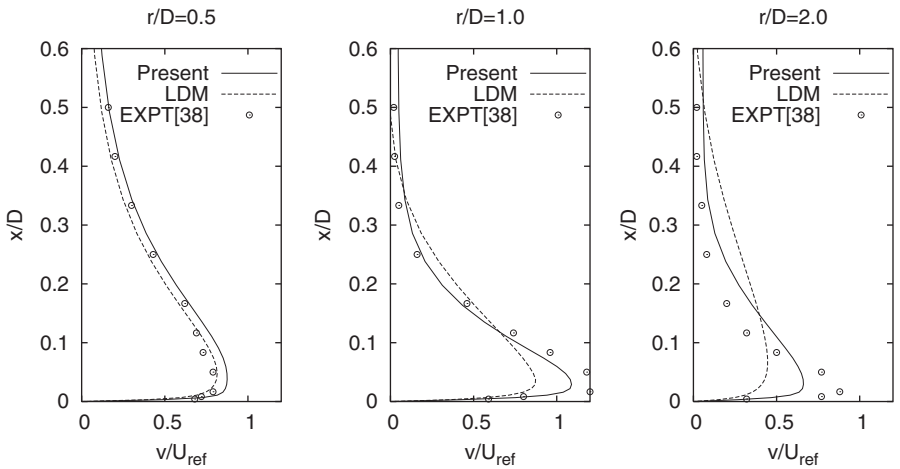

Figure 14. Mean velocity profiles at selected locations for jet flow.

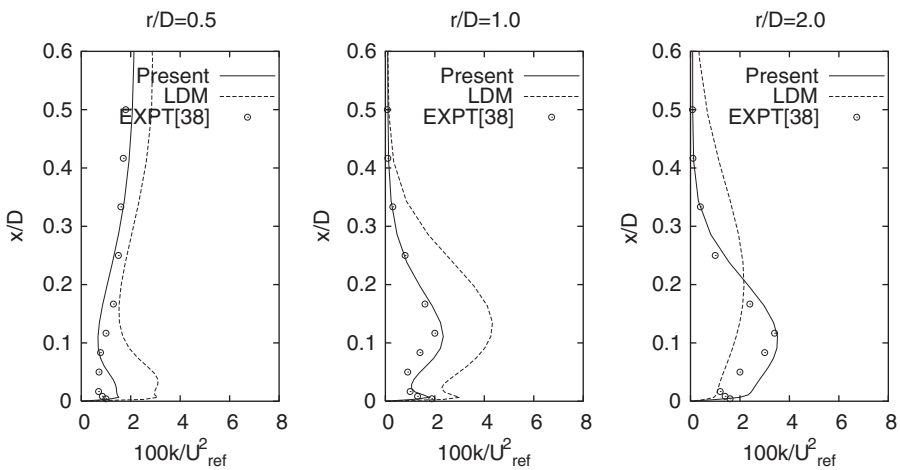

Figure 15. Kinetic energy profiles at selected locations for jet flow.

DOI: 10.1002/fld

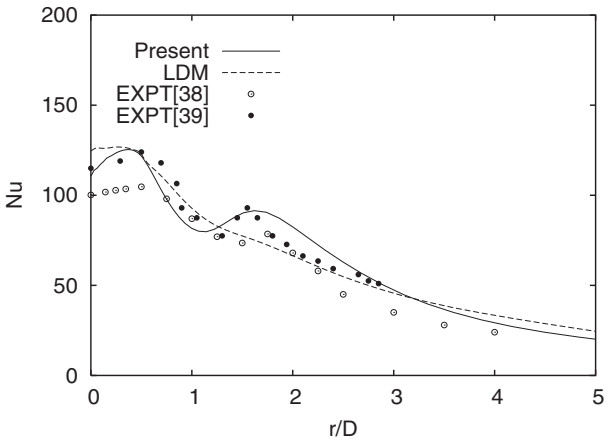

Figure 16. Nusselt number distribution on the impingement wall for jet flow.

boundary condition [38]. A 80×64 grid is adopted with a heavy clustering near the wall. The maximum height of the first near-wall grid node is at $y^+ < 1.0$. Note that the turbulent heat flux is estimated using the Boussinesq approximation and the turbulent Prandtl number $\sigma_t = 0.9$ [3].

Numerical and experimental profiles of the radial velocity are compared in Figure 14. Good agreement between the present model and the experimental data is retained, in contrast to the LDM. However, both models underpredict the spreading rate in the wall jet boundary layer where the flow is accelerated. Computations of Ashforth-Frost and Jambunathan [38] show the similar behaviour in the wall jet layer.

Profiles for the turbulence kinetic energy are shown in Figure 15. Clearly, agreement with experimental data is acceptable with the present model. Figure 16 displays the comparison of the predicted Nusselt number to the experiments. The distance from the symmetry axis is normalized by the diameter of the jet. As is evident, both models predict the Nu distribution with reasonable accuracies.

4. CONCLUSIONS

The simplified v^2–f model is susceptible to the near-wall and LRN effects emanating from the physical requirements. Avoiding the free-stream dependency, the new formulation leads to solving the governing equations in an uncoupled and much more robust way than that of the LDM. The potential importance of the elliptic relaxation function is conspicuous. The model coefficients/functions depend nonlinearly on both the mean strain rate and vorticity invariants that preserve the anisotropic characteristic of turbulence. Consequently, the model is capable of evaluating the flow cases entangling separation and reattachment. Contrasting the predicted results with measurements demonstrates that the present model offers considerable improvement over the LDM.

DOI: 10.1002/fld

NOMENCLATURE

C_f	friction coefficient
C_μ	eddy viscosity coefficient
f	elliptic relaxation parameter
h	channel/step height
k	turbulent kinetic energy
L	characteristic length scale
P	production of turbulent kinetic energy
Re	Reynolds number
Re_T	turbulent Reynolds number
S	mean strain-rate
T_t	realizable time scale
T_u	turbulence intensity
t	time
$-\rho\overline{u_i u_j}$	Reynolds stresses
u_i	mean velocity components
U_{ref}	reference velocity
$\overline{v}^2$	squared velocity scale
W	mean vorticity
x, y	Cartesian co-ordinates
y^+	non-dimensional normal distance from the solid surface

Greek letters

δ	half-width of the channel
δ_{ij}	Kronecker's delta
ε	turbulent dissipation
μ, μ_T	molecular and eddy viscosities
$\nu = \mu/\rho$	molecular kinematic viscosity
ρ	density
σ	turbulent Prandtl number
τ	shear stress

REFERENCES

1. Kim J. On the structure of pressure fluctuations in simulated turbulent channel flow. *Journal of Fluid Mechanics* 1989; **205**:421–451.
2. So RMC, Sarkar A, Gerodimos G, Zhang J. A dissipation rate equation for low-Reynolds number and near-wall turbulence. *Theoretical and Computational Fluid Dynamics* 1997; **9**:47–63.
3. Jones WP, Launder BE. The calculation of low-Reynolds number phenomena with a two-equation model of turbulence. *International Journal of Heat and Mass Transfer* 1973; **16**:1119–1130.
4. Launder BE, Sharma BI. Application of the energy dissipation model of turbulence to the calculation of flow near a spinning disc. *Letters in Heat and Mass Transfer* 1974; **1**:131–138.
5. Chien K-Y. Predictions of channel and boundary layer flows with a low-Reynolds number turbulence model. *AIAA Journal* 1982; **20**:33–38.
6. Patel VC, Rodi W, Scheuerer G. Turbulence models for near-wall and low Reynolds number flow: a review. *AIAA Journal* 1985; **23**:1308–1319.
7. Mansour NN, Kim J, Moin P. Near-wall k–ε turbulence modeling. *AIAA Journal* 1989; **27**:1068–1073.

DOI: 10.1002/fld

8. Nagano T, Tagawa M. An improved k–ε model for boundary layer flows. *Journal of Fluids Engineering* 1990; **112**:33–39.
9. Yang Z, Shih TH. New time scale based k–ε model for near-wall turbulence. *AIAA Journal* 1991; **29**:1337–1340.
10. Nagano Y, Kondoh M, Shimada M. Multiple time scale turbulence model for wall and homogeneous flows based on direct numerical simulations. *International Journal of Heat and Fluid Flow* 1997; **18**:346–359.
11. Goldberg U, Apsley D. A wall-distance-free low *Re* k–ε turbulence model. *Computer Methods in Applied Mechanics and Engineering* 1997; **145**:227–238.
12. Hwang CB, Lin CA. Improved low-Reynolds number k–$\tilde{\varepsilon}$ model based on direct numerical simulation data. *AIAA Journal* 1998; **36**:38–43.
13. Chen WL, Lien FS, Leschziner MA. Nonlinear eddy viscosity modelling of transitional boundary layers pertinent to turbomachine aerodynamics. *International Journal of Heat and Fluid Flow* 1997; **19**:297–306.
14. Rahman MM, Siikonen T. Improved low-Reynolds-number k–$\tilde{\varepsilon}$ model. *AIAA Journal* 2000; **38**:1298–1300.
15. Rahman MM, Siikonen T. Low-Reynolds-number k–$\tilde{\varepsilon}$ model with enhanced near-wall dissipation. *AIAA Journal* 2002; **40**:1442–1464.
16. Rahman MM, Siikonen T. Near-wall turbulence modelling with enhanced dissipation. *International Journal for Numerical Methods in Fluids* 2003; **42**:979–997.
17. Rahman MM, Siikonen T. A two-equation model with relevance to near-wall turbulence. *Far East Journal of Applied Mathematics* 2004; **17**:1–26.
18. Rahman MM, Siikonen T. Low-Reynolds number k–ε model for near-wall flow. *International Journal for Numerical Methods in Fluids* 2005; **47**:325–338.
19. Lumley JL. Computational modeling of turbulent flows. *Advances in Applied Mechanics* 1978; **18**:124–176.
20. Durbin PA. Near-wall turbulence closure modeling without damping functions. *Theoretical Computational Fluid Dynamics* 1991; **3**:1–13.
21. Durbin PA. Separated flow computations with k–ε–v^2 model. *AIAA Journal* 1995; **33**:659–664.
22. Lien FS, Durbin PA. Nonlinear k–ε–v^2 modeling with application to high-lift. *Proceedings of the Summer Program 1996*, Stanford University, 1996; 5–22.
23. Lien FS, Kalitzin G. Computations of transonic flow with the v^2–f turbulence model. *International Journal of Heat and Fluid Flow* 2001; **22**:53–61.
24. Kalitzin G. Numerical issues and free stream behavior of the v^2–f model. *Annual Research Briefs 2004*, Center for Turbulence Research, Stanford University, 2004; 55–62.
25. Mansour NN, Kim J, Moin P. Reynolds-stress and dissipation-rate budgets in a turbulent channel flow. *Journal of Fluid Mechanics* 1988; **194**:15–44.
26. Manceau R, Wang M, Laurence D. Inhomogeneity and anisotropy effects on the redistribution term in Reynolds-averaged Navier–Stokes modelling. *Journal of Fluid Mechanics* 2001; **438**:307–338.
27. Durbin PA, Speziale CG. Local anisotropy in strained at high Reynolds numbers. *Journal of Fluids Engineering* 1991; **113**:707–709.
28. Durbin PA. A Reynolds-stress model for near-wall turbulence. *Journal of Fluid Mechanics* 1993; **249**:465–498.
29. Ahn JW, Park TS, Sung HJ. Application of a near-wall turbulence model to the flows over a step with inclined wall. *International Journal of Heat and Fluid Flow* 1997; **18**:209–217.
30. Rahman MM, Rautaheimo P, Siikonen T. Numerical study of turbulent heat transfer from a confined impinging jet using a pseudo-compressibility method. In *Second International Symposium on Turbulence*, *Heat and Mass Transfer*, Hanjalic K, Peeters TWJ (eds). Delft University Press: Delft, The Netherlands, 1997; 511–520.
31. Rahman MM, Siikonen T. An artificial compressibility method for incompressible flows. *Numerical Heat Transfer*, *Part B* 2001; **40**:391–409.
32. Roe PL. Approximate Riemann solvers, parameter vectors, and difference schemes. *Journal of Computational Physics* 1981; **43**:357–372.
33. Lombard C, Bardina J, Venkatapathy E, Oliger J. Multi-dimensional formulation of CSCM—an upwind flux difference eigenvector split method for the compressible Navier–Stokes equations. *Sixth AIAA Computational Fluid Dynamics Conference*, *AIAA Paper 83-1895-CP*, 1983; 649–664.
34. Jameson A, Yoon S. Multigrid solution of the Euler equations using implicit schemes. *AIAA Journal* 1986; **24**:1737–1743.
35. Savill AM. Some recent progress in the turbulence modeling of by-pass transition. *Near-Wall Turbulent Flows*, So RMC, Speziale CG, Launder BE (eds). Elsevier: Amsterdam, 1993; 829–848.
36. Driver DM, Seegmiller HL. Features of a reattaching turbulent shear layer in divergent channel flow. *AIAA Journal* 1985; **23**:163–171.

DOI: 10.1002/fld

37. Buice C, Eaton JK. Experimental investigation of flow through an asymmetric plane diffuser. *Report TSD-107*, Department of Mechanical Engineering, Thermoscience Division, Stanford University, California, CA, 1997.
38. Ashforth-Frost S, Jambunathan K. Numerical prediction of semiconfined jet impingement and comparison with experiment. *International Journal for Numerical Methods in Fluids* 1996; **23**:295–306.
39. Ashforth-Frost S, Jambunathan K, Whitney CF, Ball SJ. Heat transfer from a flat plate to a turbulent axisymmetric impinging jet. *Proceedings of the Institution of Mechanical Engineers*, *Part C*: *Journal of Mechanical Engineering Science* 1997; **211**(2):167–172.

DOI: 10.1002/fld